



# CHORUS

This is the accepted manuscript made available via CHORUS. The article has been published as:

## Observation of a Magnetopiezoelectric Effect in the Antiferromagnetic Metal $\text{EuMnBi}_2$

Y. Shiomi, H. Watanabe, H. Masuda, H. Takahashi, Y. Yanase, and S. Ishiwata

Phys. Rev. Lett. **122**, 127207 — Published 29 March 2019

DOI: [10.1103/PhysRevLett.122.127207](https://doi.org/10.1103/PhysRevLett.122.127207)

# Observation of Magnetopiezoelectric Effect in Antiferromagnetic Metal EuMnBi<sub>2</sub>

Y. Shiomi<sup>1,2,3</sup>, H. Watanabe<sup>4</sup>, H. Masuda<sup>1</sup>, H. Takahashi<sup>1</sup>, Y. Yanase<sup>4</sup>, and S. Ishiwata<sup>1,5</sup>

<sup>1</sup> *Department of Applied Physics and Quantum-Phase Electronics Center (QPEC),  
University of Tokyo, Hongo, Tokyo 113-8656, Japan*

<sup>2</sup> *RIKEN Center for Emergent Matter Science (CEMS), Wako 351-0198, Japan*

<sup>3</sup> *Department of Basic Science, University of Tokyo, Meguro, Tokyo 153-8902, Japan*

<sup>4</sup> *Department of Physics, Kyoto University, Kyoto 606-8502, Japan and*

<sup>5</sup> *PRESTO, Japan Science and Technology Agency, Kawaguchi 332-0012, Japan*

(Dated: March 11, 2019)

We have experimentally studied a magnetopiezoelectric effect predicted recently for magnetic metals with low crystal symmetries. In EuMnBi<sub>2</sub> with antiferromagnetic Mn moments at 77 K, dynamic displacements emerge along the  $a$  direction upon application of ac electric fields in the  $c$  direction, and increase in proportion to the applied electric fields. Such displacements are not observed along the  $c$  direction of EuMnBi<sub>2</sub> or EuZnBi<sub>2</sub> with nonmagnetic Zn ions. As temperature increases from 77 K, the displacement signals decrease and disappear at about 200 K, above which electric conduction changes from coherent to incoherent. These results demonstrate the emergence of the magnetopiezoelectric effect in a magnetic metal lacking inversion and time-reversal symmetries.

Piezoelectric effects that allow conversion between electric and mechanical stresses are essential for a variety of applications, such as sensors, transducers, and actuators [1, 2]. To date, many examples of piezoelectric materials *e.g.* quartz [3], bones [4], barium titanates [5], lead zirconate titanates [6], and alkaline niobates [7] have been found; all the materials are insulators. Indeed, the search for piezoelectric materials has been carried out with insulators and semiconductors, since for metals, static electrical polarization is screened by conduction electrons and ceases to be well defined [8]. Nevertheless, recent advances in the study of polar metals with long-range ordered dipoles [8–10] have promised the evolution of time-dependent strain in response to ac electric currents in noncentrosymmetric metals [11].

Magnetopiezoelectric effect (MPE), which was theoretically predicted very recently [11–13], has a potential to realize a strain response to electric currents in metals. For magnetic metals that simultaneously break time-reversal and space-inversion symmetries, the breaking of the symmetries results in dynamical distortion in response to ac electric currents [11–13]. Electric currents induce an electronic nematic order in metals lacking inversion and time-reversal symmetries [12]; the nematic order accompanies the modulation of Fermi surfaces, which in turn leads to a structural deformation through electron-lattice couplings. The MPE thereby requires Fermi surfaces, and interestingly, is expected to be free from screening effects unlike conventional piezoelectric effects [12, 13]. Also, the MPE can be viewed as a generalization of magnetoelectric responses in insulators, and its relation to Berry phase effects has been discussed [11]. Hence, the MPE can be a promising probe for hidden electronic properties such as nematicity and Berry curvature in low-symmetry metals.

Dynamic strains caused by ac electric currents in the MPE is apparently a metallic analog of the inverse piezoelectric effect, but the MPE differs from the conventional piezoelectric effect in terms of symmetry [11–13]. In

the MPE, both time-reversal and space-inversion symmetries need to be broken, and hence the MPE occurs only in magnetically ordered states. In contrast, the conventional piezoelectric effect respects time-reversal symmetry. From the symmetry argument, the conventional piezoelectricity does not arise in magnetopiezoelectric metals where magnetic order breaks space inversion symmetry [12].

In this letter, we experimentally study the MPE for antiferromagnetic metal EuMnBi<sub>2</sub> [14–18]. In the antiferromagnetic state, EuMnBi<sub>2</sub> has the same crystal symmetry as hole-doped BaMn<sub>2</sub>As<sub>2</sub>, the MPE of which was discussed theoretically [12]. As shown in Fig. 1(a), antiferromagnetic EuMnBi<sub>2</sub> possesses the  $D_{2d}$  symmetry [19, 20], which allows the magnetopiezoelectric response given by  $\varepsilon_{xy} = e_{zxy}E_z$  [12]. Namely, an electric field along the  $z$  axis ( $E_z$ ) induces a stress along the [110] direction ( $\varepsilon_{xy}$ ) which leads to deformation from the tetragonal to orthorhombic lattice [21] [see Supplemental Material (SM) [22]]. Here,  $e_{zxy}$  is a magnetopiezoelectric coefficient, a measure of the piezoelectric conversion efficiency.

We employ laser Doppler vibrometry [27–30] in a low-temperature environment to detect very small magnetopiezoelectric signals. The laser Doppler vibrometry enables non-contact detection of sub-pm-level vibrations even for thin films [29, 30] and microstructures [31], by measuring the Doppler frequency shift of the scattered light from the sample using a two-beam laser interferometer [Fig. 1(b)]. By applying ac electric fields along the  $c$  axis of EuMnBi<sub>2</sub>, we have observed dynamic displacements satisfying the relation  $\varepsilon_{xy} = e_{zxy}E_z$  at 77 K. Such displacements are not observed for a paramagnetic analogue EuZnBi<sub>2</sub>. The dynamic displacements observed in EuMnBi<sub>2</sub> decreases with increasing temperature, and becomes undetectable levels above  $\sim 200$  K, the crossover temperature of coherent to incoherent (hopping-like) conduction. The present results provide experimental evidence of the MPE, and also reveal that the laser Doppler vibrometry is a useful probe of the nematicity which has

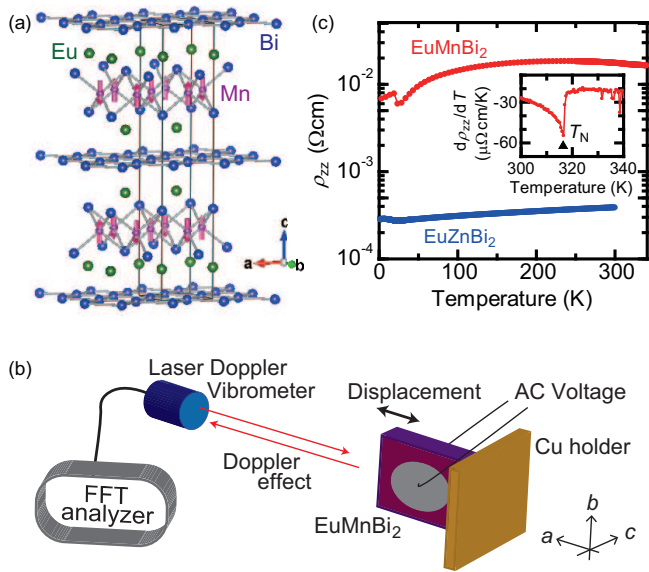


FIG. 1: (Color online.) (a) Schematic illustration of crystal structure for  $\text{EuMnBi}_2$ , together with the magnetic structure of Mn ions below the antiferromagnetic transition temperature ( $T_N$ ) [19, 20]. (b) Schematic illustration of measurement setup for the magnetopiezoelectric effect. (c) Temperature dependence of interlayer resistivity  $\rho_{zz}$  for  $\text{EuMnBi}_2$  and  $\text{EuZnBi}_2$ . The inset shows temperature derivative of resistivity for  $\text{EuMnBi}_2$  around  $T_N (= 315 \text{ K})$ . See SM [22] for inplane resistivity  $\rho_{xx}$  of  $\text{EuMnBi}_2$ .

been reported *e.g.* in cuprate superconductors [32–37], iron-based superconductors [21, 38], and heavy-electron systems [39–42].

Single crystals of  $\text{EuMnBi}_2$  and  $\text{EuZnBi}_2$  were grown by a Bi-flux method according to the papers reported by some of the present authors [15, 16]. Plate-like single crystals of  $\text{EuMnBi}_2$  with the size of  $3 \times 3 \times 1 \text{ mm}^3$  were fixed to a copper sample holder using GE varnish. On the largest planes corresponding to the  $c$  planes, voltage electrodes were formed using conductive silver pastes, as illustrated in Fig. 1(b). While applying kHz-range ac voltages to the samples along the  $c$  direction, time-dependent displacements generating along the  $a$  direction were measured using a laser Doppler vibrometer combined with a fast Fourier transform (FFT) analyzer [27–30] [Fig. 1(b)]. A red laser is directed at the surface of  $\text{EuMnBi}_2$ , and the vibration velocity of the sample is extracted from the Doppler shift of the reflected laser. The observed velocity was then numerically integrated with respect to time using the FFT analyzer, to obtain the vibration amplitude of the sample. With an objective lens, the laser spot diameter is set to be less than 100 micron, which can be smaller than domain sizes of bulk antiferromagnets [43]. Low temperature experiments were conducted with a nitrogen optistat having a quartz window.

First, we show temperature dependence of interlayer resistivity  $\rho_{zz}$  for  $\text{EuMnBi}_2$  and  $\text{EuZnBi}_2$  in Fig. 1(c).

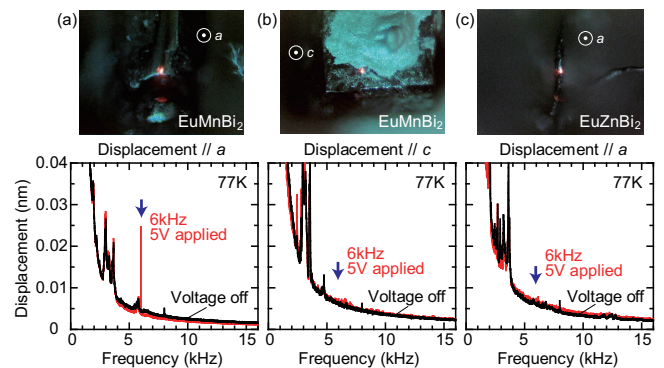


FIG. 2: (Color online.) Frequency dependence of displacement signals measured at 77 K with (red color) and without (black color) voltage application to (a), (b)  $\text{EuMnBi}_2$  and (c)  $\text{EuZnBi}_2$  samples. Here, the voltage of 6-kHz frequency and 5-V amplitude (10-V peak-to-peak amplitude) was applied along the  $c$  direction of the samples. The displacement along the  $a$  direction was measured for (a)  $\text{EuMnBi}_2$  and (c)  $\text{EuZnBi}_2$ , while that along the  $c$  direction was measured for  $\text{EuMnBi}_2$  in (b). In the top panels, sample pictures are also shown; red points correspond to the laser spots.

Here  $\rho_{zz}$  was measured by a four-terminal method on bar-shaped samples with a typical dimension of  $\sim 1.5 \text{ mm}$  in length along the  $c$  axis and  $\sim 0.4 \times 0.4 \text{ mm}^2$  in cross section [15] (see also SM [22]). As temperature decreases from 340 K,  $\rho_{zz}$  of  $\text{EuMnBi}_2$  exhibits a broad maximum at about 200 K, and decreases gently. Such a crossover from non-metallic ( $d\rho_{zz}/dT < 0$ ) to metallic ( $d\rho_{zz}/dT > 0$ ) interlayer transport has been reported in isostructural  $\text{SrMnBi}_2$  [44] and other anisotropic layered metals [45–50]. The crossover temperature is similar to  $\text{SrMnBi}_2$  ( $\sim 200 \text{ K}$ ) [44], where the interlayer transfer energy was estimated to be  $\approx 17 \text{ meV}$ . Because of anisotropic Fermi surfaces, hopping-type conduction across blocking layers is dominant at high temperatures, whereas at low temperatures, the system behaves as an anisotropic three-dimensional metal and the transport becomes metallic. In the coherent transport regime, the conductivity is determined by a scattering time (quasi-particle lifetime) and the Fermi velocity [46], but such a band picture is not valid in the incoherent regime. In contrast to the case of  $\text{EuMnBi}_2$ ,  $\rho_{zz}$  of  $\text{EuZnBi}_2$  is metallic ( $d\rho_{zz}/dT > 0$ ) in the entire temperature regime in Fig. 1(c), which reflects weaker anisotropy of  $\text{EuZnBi}_2$  than  $\text{EuMnBi}_2$ . At approximately 20 K,  $\rho_{zz}$  for  $\text{EuMnBi}_2$  and  $\text{EuZnBi}_2$  shows an anomaly, corresponding to magnetic transition of Eu ions [15, 16]. As shown in the inset to Fig. 1(c), the antiferromagnetic transition temperature of Mn ions in  $\text{EuMnBi}_2$  is determined to be 315 K [14] from the temperature derivative of resistivity.

We then performed measurements of the MPE for  $\text{EuMnBi}_2$  at 77 K. Figure 2 shows FFT spectra of displacements for  $\text{EuMnBi}_2$  and  $\text{EuZnBi}_2$  with and without application of voltage. In Fig. 2(a), the displacement

was measured along the  $a$  direction of  $\text{EuMnBi}_2$  while applying voltage of 6-kHz frequency to the  $c$  direction. When the voltage is off, no signals are observed at the frequency of the voltage (6 kHz); note that at low frequencies, the displacement signal diverges because the numerical integration of velocity data in the frequency domain corresponds to division of the velocity by frequency. However, when 5-V voltage of 6-kHz frequency is applied, a peak signal is clearly observed at the voltage frequency. The magnitude of the displacement at 6 kHz is 0.025 nm. Small signals observed at 2-4 kHz are unchanged by voltage application, and thereby safely ascribed to noises from the sample holder (possibly due to boiling of liquid nitrogen since the noises disappear at high temperatures in Fig. 3). See also SM [22] for the laser-position dependence and the voltage-frequency dependence of the displacement signal. Since heating effects ( $\propto E_z^2$ ) should give rise to second-harmonic signals (at 12 kHz), the clear displacement signal at the voltage frequency agrees with the MPE.

To check the consistency with the MPE, we measured displacements along the  $c$  direction of the same  $\text{EuMnBi}_2$  sample while applying ac voltage in the  $c$  direction in Fig. 2(b). When the laser direction is parallel to the voltage direction, we found that the displacement signal at the voltage frequency is smaller than the measurement limit even in the case of application of 5-V voltage. This direction dependence is consistent with the MPE expected from the symmetry in  $\text{EuMnBi}_2$  [12]; for ac voltage applied to the  $c$  direction, the distortion is expected along the [110] direction, but not along the  $c$  direction. We also confirmed that displacement signals are not observed in response to applied voltages for isostructural paramagnet  $\text{EuZnBi}_2$ , as shown in Fig. 2(c). Antiferromagnetic Mn ions are therefore necessary for the emergence of the displacement signals.

Voltage-amplitude dependence of the displacement signal is examined at 77 K in Fig. 3(a). Here, the displacement is measured in the  $a$  direction of  $\text{EuMnBi}_2$  while the amplitude of 6-kHz voltage is changed from 0 V through 5 V. At 0 V, no signal is recognized, but the signal at 6 kHz gradually increases with increasing voltage amplitudes. For 5-V voltage corresponding to  $\approx 100$  mA, the displacement reaches 0.025 nm. The 6-kHz displacement is plotted as a function of the voltage amplitude in Fig. 4(a). Obviously, the displacement at the voltage frequency increases in proportion to voltage intensity, consistent with the MPE. From a linear fit to the experimental data [dotted line in Fig. 4(a)], we noticed that there is a small offset independent of voltage application. This offset, whose magnitude is as small as 3 pm, is ascribable to experimental noises, since the measured displacement signals should include noise signals from the measurement environment in addition to the MPE.

Temperature dependence of the MPE is also informative, because the magnitude of the MPE signal depends on transport, mechanical, and magnetic properties. The displacement signal at the 6-kHz voltage fre-

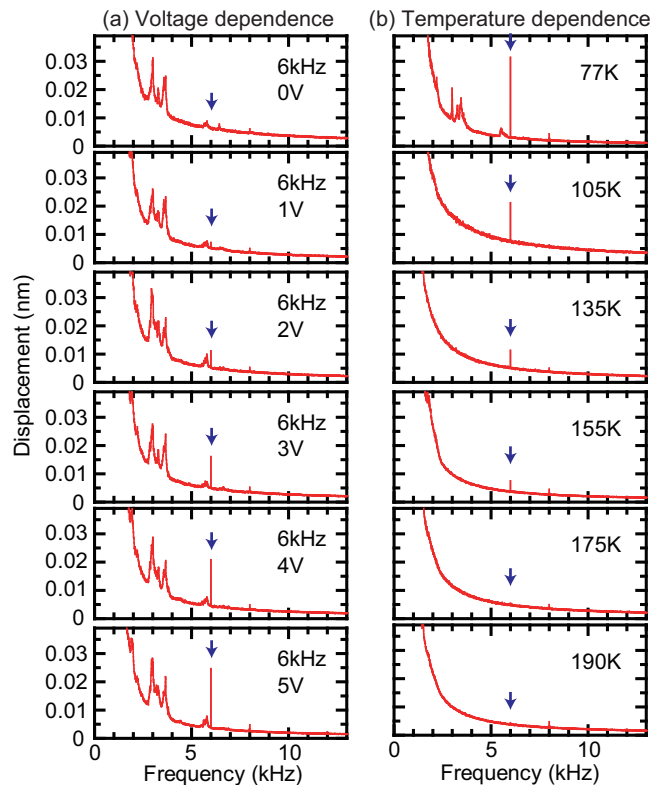


FIG. 3: (Color online.) (a) Frequency dependence of the displacement signals measured with various voltage amplitudes for  $\text{EuMnBi}_2$  at 77 K. Here, the displacements were measured along the  $a$  direction while the voltage of 6-kHz frequency was applied to the  $c$  direction. (b) Frequency dependence of the displacement signals measured for  $\text{EuMnBi}_2$  at various temperatures. Here, the displacements were measured along the  $a$  direction while the voltage of 6-kHz frequency and 5-V amplitude was applied to the  $c$  direction.

quency was thereby investigated at different temperatures in Fig. 3(b), although the data might include ambiguity because background levels inevitably change by temperature shift of the laser position. As temperature increases from 77 K, the displacement signal at 6 kHz decreases monotonically, and finally disappears at 175 K. As shown in SM [22], we confirmed that the signal also disappears at approximately 200 K for different two  $\text{EuMnBi}_2$  samples. The onset temperature of  $\sim 200$  K is much smaller than the antiferromagnetic transition temperature of  $\text{EuMnBi}_2$  (315 K), where the magnetic order breaks space inversion symmetry. Instead, the emergence of the MPE seems to be related with the crossover of incoherent to coherent conduction [Fig. 1(b)]. In the high-temperature incoherent regime, the interlayer transport is no longer dictated by the Fermi-liquid picture [46], and the MPE becomes indiscernible.

In Fig. 4(b), temperature dependence of the displacement signal observed at the voltage frequency is summarized. With increasing temperature from 77 K, the

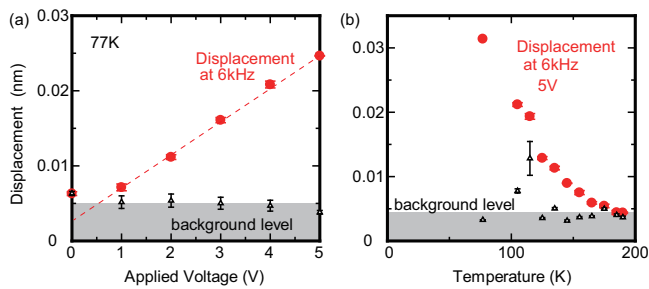


FIG. 4: (Color online.) (a) Voltage dependence of the displacement signal measured at 6 kHz (red circles). See Fig. 3(a) for raw data. The background levels (black triangles) correspond to the averaged displacements around 6 kHz without voltage application. The dotted line is guide for eyes. (b) Temperature dependence of the displacement signal measured at 6 kHz (red circles). See Fig. 3(b) for raw data. The background levels (black triangles) correspond to the averaged displacements around 6 kHz without voltage application.

displacement signal rapidly decreases almost as the inverse square of temperature. As mentioned before, the temperature dependence of the MPE signal depends on transport, mechanical, and also magnetic properties of materials, but has not been discussed in detail in the theoretical papers [11–13]. In fact, though the susceptibility of the current-induced nematic order was calculated to be proportional to scattering time [12], the temperature dependence of the displacement is apparently greater than that of interlayer conductivity [Fig. 1(c)]. Owing to the strong anisotropy in Fermi surfaces [16, 44], interlayer conductivity may not be proportional to scattering time [47]. Also, temperature change in electron-lattice couplings affects that of the MPE signal. Furthermore, the MPE signal in EuMnBi<sub>2</sub> depends also on exchange couplings between itinerant Bi-electron spins and localized Mn moments, since conduction is governed by Bi-band electrons but magnetism originates from Mn moments. The spin exchange couplings can be stronger at lower temperatures. Though the authors in the preceding theoretical papers [12, 13] discuss the MPE for antiferromagnetic metals from the symmetry argument, a microscopic model in which material parameters are taken into account will be necessary to elucidate the temperature dependence of the MPE signal in EuMnBi<sub>2</sub>.

Finally, from the experimental results at 77 K, we

estimate the magnitude of magnetopiezoelectric coefficient  $e_{zxy}$  for EuMnBi<sub>2</sub>. Using the applied voltage 5 V, the observed displacement 0.025 nm, and the sample size,  $e_{zxy}$  is calculated to be approximately 1 pC/N. Let us compare  $e_{zxy}$  of EuMnBi<sub>2</sub> with typical piezoelectric constants, since the strain response to electric fields in the MPE can be viewed as a kind of piezoelectric responses. The magnitude of  $e_{zxy}$  is 1000 times less than the piezoelectric constant for lead zirconate titanates [6], and comparable to that of quartz [3, 51]. The performance of EuMnBi<sub>2</sub> as an alternative to piezoelectric materials is thereby insufficient for device applications, but one can expect that materials with higher conductivity (scattering time) have higher magnetopiezoelectric coefficients [12]. From this perspective, anisotropic EuMnBi<sub>2</sub> ( $\rho_{zz} \approx 1 \times 10^{-2} \Omega\text{cm}$ ) is not suitable for large magnetopiezoelectric coefficients, and three-dimensional systems with isotropic Fermi surfaces *e.g.* Mn<sub>2</sub>Au [13] ( $\rho \approx 1 \times 10^{-5} \Omega\text{cm}$  [52]) may be a better choice of materials.

In summary, the MPE has been demonstrated for antiferromagnetic metal EuMnBi<sub>2</sub> using laser Doppler vibrometry that can detect tiny sample vibrations sensitively. In response to applied ac voltages in the  $c$  direction, an inplane dynamic displacement whose magnitude increases in proportion to applied voltage was observed for EuMnBi<sub>2</sub> single crystals at 77 K, whereas not for paramagnetic relative EuZnBi<sub>2</sub>. As temperature increases, the displacement signal due to voltage application decreases monotonically and disappears at approximately 200 K. This result indicates that the transport governed by coherent quasiparticles is necessary for the generation of the MPE signal. The MPE, which enables the generation of time-dependent strain in response to ac electric fields in magnetic metals, could lead to a new function in piezoelectric devices, as well as spintronic devices.

The authors thank Y. Tokura, N. Nagaosa, T. Naka-jima, and K. Harii for fruitful discussions. This work was supported by JSPS (KAKENHI No. 15H05884, No. 16K17736, No. 17H01195, No. 17H04806, No. JP18H04225, No. JP18H04215, No. 18H01178, and No. 18H04311). Y.S. was supported by JST ERATO Grant Number JPMJER1402, Japan, and H.W. and H.M. were supported by JSPS through a research fellowship for young scientists (No. JP18J23115 and No. JP16J10114, respectively).

[1] J. Tichý, J. Erhart, E. Kittinger, and J. Přívratská, *Fundamentals of Piezoelectric Sensorics: Mechanical, Dielectric, and Thermodynamical Properties of Piezoelectric Materials*, Springer-Verlag GmbH, Berlin (2010).  
 [2] D. Damjanovic, Rep. Prog. Phys. **61**, 1267 (1998).  
 [3] J. Curie and P. Curie, C. R. Acad. Sci. Paris **91**, 294 (1880).  
 [4] M. Minary-Jolandan and M.-F. Yu, Nanotechnology **20**,

085706 (2009).  
 [5] A. von Hippel, Rev. Mod. Phys. **22**, 221 (1950).  
 [6] P. K. Panda and B. Sahoo, Ferroelectrics **474**, 128 (2015).  
 [7] Y. Saito, H. Takao, T. Tani, T. Nonoyama, K. Takatori, T. Homma, T. Nagaya and M. Nakamura, Nature **432**, 84 (2004).  
 [8] T. H. Kim *et al.* Nature **533**, 68-72 (2016).

- [9] D. Puggioni and J. M. Rondinelli, *Nat. Commun.* **5**: 3432 (2014).
- [10] Y. Shi *et al.* *Nat. Mater.* **12**, 1024-1027 (2013).
- [11] D. Varjas, A. G. Grushin, R. Ilan, and J. E. Moore, *Phys. Rev. Lett.* **117**, 257601 (2016).
- [12] H. Watanabe and Y. Yanase, *Phys. Rev. B* **96**, 064432 (2017).
- [13] H. Watanabe and Y. Yanase, *Phys. Rev. B* **98**, 245129 (2018).
- [14] A. F. May, M. A. McGuire, and B. C. Sales, *Phys. Rev. B* **90**, 075109 (2014).
- [15] H. Masuda *et al.* *Sci. Adv.* **2**, e1501117 (2016).
- [16] H. Masuda, H. Sakai, M. Tokunaga, M. Ochi, H. Takahashi, K. Akiba, A. Miyake, K. Kuroki, Y. Tokura, and S. Ishiwata, *Phys. Rev. B* **98**, 161108(R) (2018).
- [17] Y. Iwasaki and T. Morinari, *J. Phys. Soc. Jpn.* **87**, 033706 (2018).
- [18] M. Chinotti, A. Pal, W. J. Ren, C. Petrovic, and L. Degiorgi, *Phys. Rev. B* **94**, 245101 (2016).
- [19] Y. F. Guo, A. J. Princep, X. Zhang, P. Manuel, D. Khalyavin, I. I. Mazin, Y. G. Shi, and A. T. Boothroyd, *Phys. Rev. B* **90**, 075120 (2014).
- [20] H. Masuda, H. Sakai, H. Takahashi, Y. Yamasaki, A. Nakao, T. Moyoshi, H. Nakao, Y. Murakami, T. Arima, and S. Ishiwata, in preparation.
- [21] S. Kasahara *et al.* *Nature* **486**, 382 (2012).
- [22] See Supplemental Material [url] for additional experimental results, which includes Refs. [23-26].
- [23] Jie-Fang Li, P. Moses, and D. Viehland, *Rev. Sci. Instrum.* **66**, 215 (1995).
- [24] A. L. Kholkin, Ch. Wütchrich, D. V. Taylor, and N. Setter, *Rev. Sci. Instrum.* **67**, 1935 (1996).
- [25] A. W. Tyler, A. P. Mackenzie, S. NishiZaki, and Y. Maeno, *Phys. Rev. B* **58**, R10107(R) (1998).
- [26] I. Terasaki, Y. Sasago, and K. Uchinokura, *Phys. Rev. B* **56**, R12685(R) (1997).
- [27] Y. Shiomi, T. Akiba, H. Takahashi, and S. Ishiwata, *Adv. Electron. Mater.* 1800174 (2018).
- [28] R. Herdier, D. Jenkins, E. Dogheche, D. Rèmesiens, and M. Sulc, *Rev. Sci. Instrum.* **77**, 093905 (2006).
- [29] L. N. McCartney, L. Wright, M. G. Cain, J. Crain, G. J. Martyna, and D. M. Newns, *J. Appl. Phys.* **116**, 014104 (2014).
- [30] S. Shetty, J. I. Yang, J. Stitt, and S. Trolier-McKinstry, *J. Appl. Phys.* **118**, 174104 (2015).
- [31] Y.-J. Seo, K. Harii, R. Takahashi, H. Chudo, K. Oyanagi, Z. Qiu, T. Ono, Y. Shiomi, and E. Saitoh, *Appl. Phys. Lett.* **110**, 132409 (2017).
- [32] Y. Kohsaka *et al.* *Science* **315**, 1380 (2007).
- [33] M. J. Lawler *et al.* *Nature* **466**, 347 (2010).
- [34] V. Hinkov, D. Haug, B. Fauque, P. Bourges, Y. Sidis, A. Ivanov, C. Bernhard, C. T. Lin, and B. Keimer, *Science* **319**, 597 (2008).
- [35] Y. Ando, K. Segawa, S. Komiyama and A. N. Lavrov, *Phys. Rev. Lett.* **88**, 137005 (2002).
- [36] R. Daou *et al.* *Nature* **463**, 519 (2010).
- [37] A. Damascelli, Z. Hussain, and Z. -X. Shen, *Rev. Mod. Phys.* **75**, 473 (2003).
- [38] J.-H. Chu, J. G. Analytis, K. D. Greve, P. L. McMahon, Z. Islam, Y. Yamamoto, and I. R. Fisher, *Science* **329**, 824 (2010).
- [39] R. Okazaki, T. Shibauchi, H. J. Shi, Y. Haga, T. D. Matsuda, E. Yamamoto, Y. Onuki, H. Ikeda, and Y. Matsuda, *Science* **331**, 439 (2011).
- [40] S. Tonegawa, K. Hashimoto, K. Ikada, Y.-H. Lin, H. Shishido, Y. Haga, T. D. Matsuda, E. Yamamoto, Y. Onuki, H. Ikeda, Y. Matsuda, and T. Shibauchi, *Phys. Rev. Lett.* **109**, 036401 (2012).
- [41] H. Ikeda, M.-T. Suzuki, R. Arita, T. Takimoto, T. Shibauchi, and Y. Matsuda, *Nat. Phys.* **8**, 528 (2012).
- [42] K. Matsubayashi, T. Tanaka, A. Sakai, S. Nakatsuji, Y. Kubo, and Y. Uwatoko, *Phys. Rev. Lett.* **109**, 187004 (2012).
- [43] M. Fiebig, D. Fröhlich, S. Leute, and R. V. Pisarev, *J. Appl. Phys.* **83**, 6560 (1998).
- [44] Y. J. Jo, J. Park, G. Lee, M. J. Eom, E. S. Choi, J. H. Shim, W. Kang, and J. S. Kim, *Phys. Rev. Lett.* **113**, 156602 (2014).
- [45] K. Yoshida, Y. Maeno, S. Nishizaki, S. Ikeda, and T. Fujita, *J. Low. Temp. Phys.* **105**, 1593 (1996).
- [46] T. Valla *et al.* *Nature* **417**, 627 (2002).
- [47] D. B. Gutman and D. L. Maslov, *Phys. Rev. Lett.* **99**, 196602 (2007).
- [48] I. Terasaki, Y. Sasago, and K. Uchinokura, *Phys. Rev. B* **56**, R12685(R) (1997).
- [49] S. M. Loureiro, D. P. Young, R. J. Cava, R. Jin, Y. Liu, P. Bordet, Y. Qin, H. Zandbergen, M. Godinho, M. Nunez-Regueiro, and B. Batlogg, *Phys. Rev. B* **63**, 094109 (2001).
- [50] I. Tsukada, T. Yamamoto, M. Takagi, T. Tsubone, S. Konno, and K. Uchinokura, *J. Phys. Soc. Jpn.* **70**, 834-840 (2001).
- [51] Y.-M. You *et al.* *Science* **357**, 306 (2017).
- [52] S. Yu. Bodnar, L. Šmejkal, I. Turek, T. Jungwirth, O. Gomonay, J. Sinova, A. A. Sapozhnik, H.-J. Elmers, M. Kläui, and M. Jourdan, *Nat. Commun.* **9**, 348 (2018).